3D printed mould inserts by DLP

Pursuing the limit of AM-manufactured resolution while maintaining dimensional accuracy and repeatability

Authors:
Silas Thorn Jensen - s163066
Jacob-Gustav Bertelsen - s163115

Hand-in date:
3^{rd} of February 2019

Supervisors:
Yang Zhang
Ali Davoudinejad
Dongya Li
Francesco Regi
Macarena Mendez Ribo

DTU Mechanical Engineering
Department of Mechanical Engineering

Contents

Abstract

1 Introduction

Pixel is a portmanteau of the words "picture" and "element". 2D Computer generated images are build from these pixel, with resolution being increased with the amount of pixels pr. image. Pixels are square, with equal X and Y dimensions. Voxel is a portmanteau of "volume" and "pixel", used in 3D computer generated images. The added Z dimension is a variable in the additive manufacturing method refered to as DLP.

2 Milestone 1

2.1 Safety and health

SDS on the materials warn respiratory complications when working without proper ventilation. This prompted the initiative to early in the process install exhaust ventilation in the working environment.
Prior to this work, resin leftover from the vat was removed using a spoon. Safety regarding pouring material back and to ease this process step, has been made better using a pump-mechanism to suction up leftover resin for re-use.

2.2 DTU DLP

This section will focus on the specifications of DTU DLP.

CPM-SDSK-2310S-EQN -¿ Servo motor from Clear Path

2.3 Grey-scale anti-aliasing

Grey-scale anti-aliasing is a method of manipulating sub pixel structures when doing additive manufacturing with a DLP. For computer graphics anti-aliasing is a commonly used method to make jagged edges appear smooth by adding gradient between a figure and the background. For a black and white images or fonts, this method uses gradients of grey scale to create the effect of a smooth boundary. See Figure 2.2.

Figure 2.1: Example of Grey-Scale Anti-Aliasing using the font Times New Roman.

The Autodesk Ember 3D Printer team researched the influence of grey scale on voxel growth. They found that grey scale allows influence on the voxel size, by changing the intensity of exposure, see Figure ??. This opens up for sub pixel geometrical feature manipulation, by rounding corners on circular features and remove jagged edges from slopes. Richard Greene's work for Ember also shows how the resolution of the projector influences the amount of grey values can be used as input for manipulating sub pixel features.

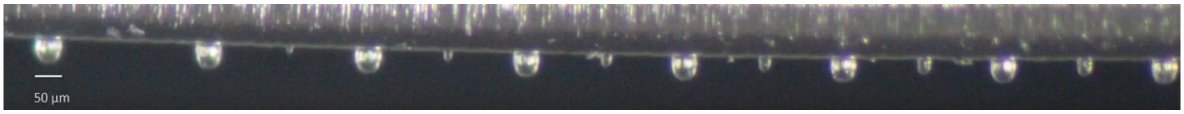

Figure 2.2: From left to right is the black to white transition.
Each gray scale voxel is printed with a complete voxel next to it for comparison.

Given the specification of the light engine used in the DTU DLP, the Luxbeam_LRS_WQ_UG, as long as the exposure time is above 4046 μ-seconds 8-bit color depth should be attainable. 8-bit color depth allows for up to 256 different grey values for manipulating pixel size. Theoretically this should allow for manipulation of geometrical features of up to 1/256 of a pixel size. However, there is an unspecified threshold for darkest grey values, where no voxel growth occurs. This threshold value creates an undefined array of grey values that can be used to create sub pixel features. The stability of the entire DLP DTU manufacturing system becomes even more crucial for obtaining expanded control of sub pixel geometrical features, as slight variance makes results unreliable.

A range of different methods for grey scale anti aliasing are possible. These methods are used for computer graphics. These methods fall under the categori called ”supersampling”. Supersampling is a method used especially in videogames or animated movies, where color samples are taken at several instances around each pixel, and an average color value is calculated creating a smoother transition between pixel of different color. The number of samples influence the perceived quality of the output, but also increases the amount of computer processing used to calculate and average the different values which for 3D printing would resolve in slower slicing of layers. Supersampling of voxels makes it possible of having grey scale occur in both X, Y and Z directions. In Figure 2.3 the quality difference between sampling 16 voxels and 64 voxels is evident. However for 64 voxel samples the processing time increases drastically.

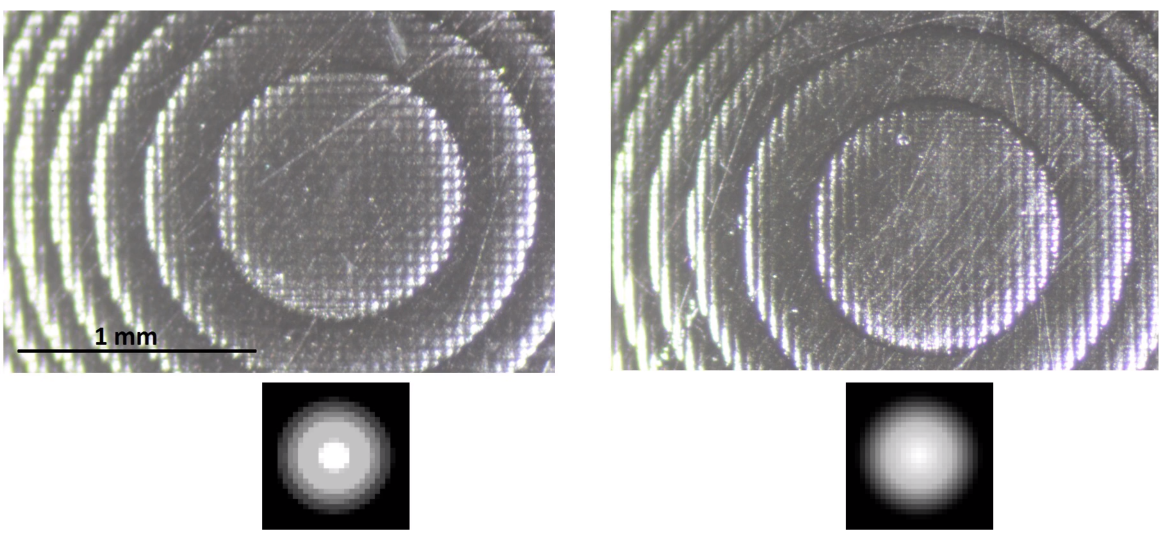

Figure 2.3: Left: 4x Supersampling (16 voxels) vs. Right: 16x Supersampling (64 voxels)

2.4 Rapid production using polymers

One of the main methods of achieving mass production of plastic components is through injection moulding. This type of manufacturing process allows for a wide variety of plastic types to be manufactured e.g. advanced engineering materials, cheaper materials for disposable consumer goods and biocompatible materials. Metal tools from hardened steels can replicate between 100’000 to a million parts, with a relatively low production time.

One of the main problems using metal tools however is the long lead time, that in some cases can be 8+ weeks, and a high cost. This becomes problematic for small to medium sized companies, with a niche type product where long lead time can create halts in development and a high cost lowers the margin of profit [X].

A different method of rapid tooling is soft tooling. Soft tooling is often used to refer to Cast Urethane [X], a type of silicone mould that can be used for injection moulding of up to 25-50 parts. Lead time and price is lower, and this is a viable option for low replication needs. However, in order to create silicon moulds a Master has to be created first. A Master can be produced relatively fast and at a low cost if it is not for precision manufacturing purpose. A part can be printed using addtive manufacturing (FDM, SLA, SLS, etc.). But for more precise parts, the production of a Master is still expensive and timeconsuming, which means that soft tooling is often not used for precision manufacturing.

With the advancement of materials for additive manufacturing, a newer method of rapid tooling has become available coined: Direct Rapid Soft Tooling (DRST). DRST is used for 3D printed mould inserts that are capable of producing 100-1000 replications, and in some cases up to 10'000s of replications. The merit of this manufacturing methods lies in the ease with which a part can be designed utilising computer aided design software (CAD), converted into mould halves and printed via additve manufacturing to be used as inserts in injection moulding[X] cutting both cost and time.

2.4.1 Rapid precision manufacturing

Precision manufacturing for advanced surface topography is linked to friction coefficient, wear resistance, self-cleaning ability, biocompatibility, optical response, touch perception and even flavor. In this work, the focus lies on the optical response of the chosen surface.

Tooling for precision manufacturing is often a slow and cost intensive manufacturing method. Tooling for replication can be done by creating a Master with precision features, this means features in the sub-mm range, these are typically manufactured using highly advanced milling methods (μ-Machining, etching, EDM) or electrochemical deposition (CVD, PVD, etc.). These methods are both time and cost intensive. Tooling for replication can also be done using earlier mentioned methods directly to create mould halves with specific microfeatures.

This master is then replicated via. a variety of ways to create micro-injectable mould halves. The replication of a master with polymer, is usually done by compression moulding, injection moulding or hot embossing, which have different trade-offs relating to price, amount of replicas and obtainable quality.

2.4.2 DRST for Precision Manufacturing

Utilising the DLP DTU additive manufacturing machine it has been possible to reproduce freeform surfaces with precision topography for optical response...

2.5 QR-code

A QR (Quick Response)-code is a 2-Dimensional bar code used to store and quickly read encoded information [ISO/IEC, 2015]. It consists of a square array of black and white nominally square modules with three identical position finding features located at three corners as depicted in Figure 2.4. ISO/IEC18004 specifies a standard module size (X) of 4 x 4 px (pixels) with a print resolution of 300 dpi (dots pr. inch).

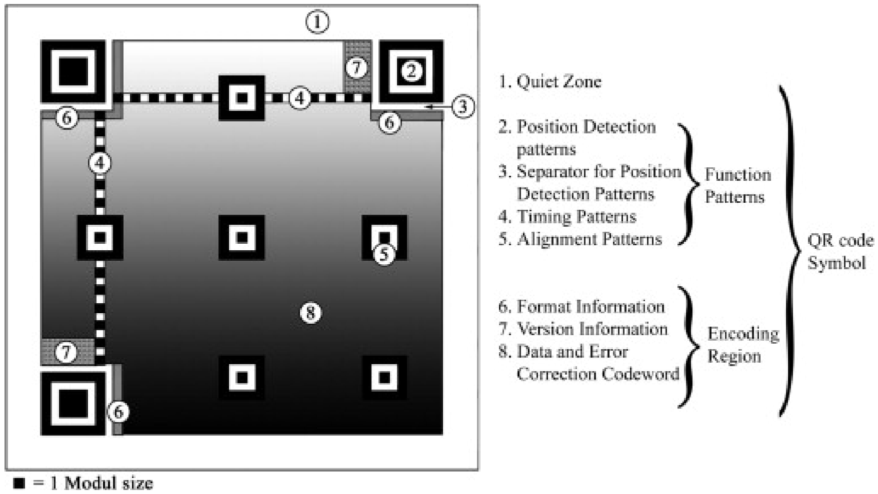

Figure 2.4: QR-code symbol overview [Tarjan et al., 2014].

The QR-code is read as a logic array with data in both horizontal and vertical patterns. A thorough sequence of error correction is applied in order to minimise failed reads which enables a QR-code to be successfully read even with defects [Denso, 2011]. The outmost region of the symbol (quiet zone, as depicted in Figure 2.4) has a significant impact on the readability of the symbol. ISO/IEC18004 specifies the quiet zone as a region with zero disturbance 4X wide on all four sides [ISO/IEC, 2015]. The reflectance of the quiet zone must correspond to the reflectance of a logic zero module.

Invented in 1994 for the Japanese automotive industry, QR-codes quickly became popular due to their fast reading times and greater information storage capacity compared to standard 1-Dimensional bar codes [Hara et al., 1998]. Application of QR-codes ranges from process chain information like product tracking, time stamp, batch number etc. to end-user features like entertainment or quick access to web-content.

2.6 Comparison of photopolymer properties in relation to normally-used materials

During the injection moulding process high pressures and temperatures are obtained to ensure low viscosity and high flow rate of the fluid plastic and make sure that all detailed features are fully replicated in the part. Normally, moulds for this process are entirely made of direct or electric discharge milled (EDM) tool steel such as P-20 or 420SS [PolyOne Cooperation, 1996]. These materials exhibit a set of very good mechanical and thermal properties such as high hardness (mainly after carburising), high stiffness, good thermal conductivity, very low thermal expansion, and very good fatigue strength [AZoM, 2012, AZoM, 2001]. This combination of properties render the injection moulding process very stable and makes it possible to minimise or even neglect certain aspects such as elastic and thermal deformation [Leo and Cuvelliez, 1996]. However, in the present case a thermosetting photopolymer insert is incorporated into a tool steel mould. Although variations occur, thermosetting photopolymers in general exhibit very different mechanical and thermal properties compared to tool steel. Table 2.1 shows a comparison of a widely used P-20 tool steel compared to different thermosetting photopolymers used for moulding purposes.

Material	**Unit**	**P-20 Tool Steel**	**E-Tool 2.0 (post cured)**	**Formlabs High Temp (post cured)**
Mechanical properties				
Density	kg/m^3	7770-7930	1050-1120	1090-1120
Tensile Strength (yield, σ_y)	MPa	827-862	-	-
Tensile Strength (ultimate, σ_{UTS})	MPa	927-1200	49.4	51.1
Compressive Strength	MPa	827-862	-	-
Elongation at Break	%	20.0	1.46	2
Tensile Modulus	GPa	204-215	4.66	3.6
Flexural Strength (ultimate)	MPa	827-862	82	106.9
Flexural Modulus	GPa	204-215	5.22	3.3
Poisson's ratio	-	0.285-0.295	-	-
Impact Strength IZOD (notched)	J/m	-	18.9	14
Impact Strength Charpy (V-notch)	J	27.1-33.9	-	-
Hardness (bulk)	Hv	303	723	-
	MPa	974	2510	-
Hardness (case)	Hv	672	723	-
	MPa	2260	2510	-
Fatigue Strength at 10^7 cycles	MPa	210	-	-
Thermal properties				
Heat capacity	J/kg.K	460	-	-
Thermal conductivity at 100°C	W/m.K	24.9	-	-
Mean coefficient of thermal expansion (20-250°C)	μstrain/°C	12.8	-	87.5
Heat deflection temperature (HDT) @ 1.8 MPa	°C	-	63	130

Table 2.1: Comparison of material properties between classical P-20 tool steel and thermosetting photopolymers. Note that the table only shows data available to the authors at present time from the manufacturers of photopolymers. All values are approximate values. If no interval is given then a representative mean value is used. [AZoM, 2001, AZoM, 2012, EnvisionTec, 2015, EnvisionTec, 2016, Formlabs, 2016, Formlabs, 2017, Granta Design Limited, 2018].

Unfortunately, Table 2.1 lacks values for certain properties of some materials. However, since the properties of the photopolymers are of relatively comparable magnitude, the table can still be used as a comparison in performance discrepancy between tool steel and photopolymers intended for tools as a general. When inspecting Table 2.1 several mechanical properties of the photopolymers differ largely from the traditional P-20 tool steel. In particular, there is more than a factor 40 difference in elastic moduli which implies dramatically higher compliance in the polymer compared to the tool steel. There is also more than a factor 20 difference in respective tensile strengths. Unfortunately, compressive strength values are not given for the photopolymers. As reflected by the values present in Table 2.1, compressive strength for metals are often similar to their tensile strength due to highly isotropic behaviour. Polymers, on the other hand do not exhibit this tendency to the same extent. As a general rule of thumb, polymers performs 20 % stronger in compression than in tension [Granta Design Limited, 2018]. Also, it can be inferred that the photopolymers are quite brittle with a elongation at break of 1-2 % compared to the 20 % of the tool steel. Therefore, brittle failure could very well be expected.

Unfortunately, very little information is given about the thermal properties of the polymers. Often, manufacturers seem to compete on heat deflection temperature (HDT) as the main indication of the thermal performance for polymers [EnvisionTec, 2016, Formlabs, 2017]. Formlabs High Temp claims more than double value of HDT compared to E-Tool 2.0 and we should therefore expect to see better performance related to thermal strains. Table 2.1 also shows more than a factor 5 difference in coefficient of thermal expansion between P-20 and Formlabs High Temp. Therefore, our mould insert will expand and contract by a relatively large amount during a heat cycle. Although no information is provided, it is safe to assume that the thermal conductivity of the photopolymers are to-three orders of magnitude lower than that of the P-20 tool steel [Granta Design Limited, 2018]. Therefore, we can expect the insert to have difficulties with dissipating the heat between injection cycles. Also, no information is provided on compressibility (Poisson's ratio) of the photopolymers. However, when comparing to other well-known thermosets like epoxies, polyurethanes, or vinyl esters it could be assumed to be 0.35-0.4[Granta Design Limited, 2018]. In fact, such a high Poisson's ratio would contribute to increase its stiffness because of the lower compressibility compared to the P20 tool steel. However, because of the large differences in elastic moduli the polymer is overall expected to exhibit much larger elastic deformation.

In conclusion there are large differences in properties between P20 tool steel and photopolymers. Relatively large elastic and thermal deformation should be expected. High pressures could result in failure due to relatively low yield and ultimate strength. Brittle failure mode should be expected. However, because of high hardness values long service life should be obtainable. Better thermal performance should be expected from Formlabs High Temp compared to the other photopolymers.

2.6.1 Heat Deflection Temperature

2.7 Elastic deformation of insert during injection

Section 2.6 illustrated many of the key differences in both mechanical and thermal performance of photopolymers compared to traditional P20 tool steel. This section seeks to analyse the effects of mechanical deformation due to the pressure applied during the injection moulding process. The effects will be analysed with both an analytic and a numerical approach.

2.7.1 Analytic approach

Key assumptions are made in order to simplify the analysis:

1. The photopolymer insert consists of a homogeneous isotropic linear elastic material and is fully constrained in x, y, and z directions by the surrounding mould half.
2. The insert is considered as a box with dimensions $x = y = 2z$
3. The surrounding mould half is mechanically stable and cannot deform.

4. The fluid polymer applies a perfectly uniform hydrostatic pressure p to the mould insert.
5. The mould insert is perfectly square and the top surface is considered perfectly flat.

Equation 2.1 shows the general linear elasticity theory (Hooke's Law) for isotropic materials in 3D. Here it is shown in compliance form:

$$\epsilon_{ij} = C_{ijkl} \cdot \sigma_{ij} \tag{2.1}$$

where i and j represents principal directions and C denotes the compliance tensor. Written in explicit form Equation 2.1 becomes:

$$\begin{Bmatrix} \epsilon_{xx} \\ \epsilon_{yy} \\ \epsilon_{zz} \\ \gamma_{xy} \\ \gamma_{yz} \\ \gamma_{zx} \end{Bmatrix} = \frac{1}{E} \begin{bmatrix} 1 & -\nu & -\nu & 0 & 0 & 0 \\ -\nu & 1 & -\nu & 0 & 0 & 0 \\ -\nu & -\nu & 1 & 0 & 0 & 0 \\ 0 & 0 & 0 & 2+2\nu & 0 & 0 \\ 0 & 0 & 0 & 0 & 2+2\nu & 0 \\ 0 & 0 & 0 & 0 & 0 & 2+2\nu \end{bmatrix} \begin{Bmatrix} \sigma_x \\ \sigma_y \\ \sigma_z \\ \tau_{xy} \\ \tau_{yz} \\ \tau_{zx} \end{Bmatrix} \tag{2.2}$$

Since the mould insert is subjected to uniformly distributed hydrostatic pressure p we can eliminate all shear components. Therefore, the 2nd order stress and strain tensors are reduced as shown:

$$[\sigma] = \begin{bmatrix} \sigma_{xx} & \cancel{\tau_{xy}} & \cancel{\tau_{xz}} \\ \cancel{\tau_{yz}} & \sigma_{yy} & \cancel{\tau_{yz}} \\ \cancel{\tau_{zx}} & \cancel{\tau_{zy}} & \sigma_{zz} \end{bmatrix} \qquad [\tau] = \begin{bmatrix} \epsilon_{xx} & \cancel{\gamma_{xy}} & \cancel{\gamma_{xz}} \\ \cancel{\gamma_{yz}} & \epsilon_{yy} & \cancel{\gamma_{yz}} \\ \cancel{\gamma_{zx}} & \cancel{\gamma_{zy}} & \epsilon_{zz} \end{bmatrix} \tag{2.3}$$

In this way Equation 2.2 can be simplified to the following:

$$\begin{Bmatrix} \epsilon_{xx} \\ \epsilon_{yy} \\ \epsilon_{zz} \end{Bmatrix} = \frac{1}{E} \begin{bmatrix} 1 & -\nu & -\nu \\ -\nu & 1 & -\nu \\ -\nu & -\nu & 1 \end{bmatrix} \begin{Bmatrix} \sigma_x \\ \sigma_y \\ \sigma_z \end{Bmatrix} \tag{2.4}$$

From Equation 2.4 it can be inferred that an applied stress in z-direction, σ_{zz}, introduces strain in the following way:

$$\epsilon_{xx} = -\frac{\nu\sigma_{zz}}{E} \qquad \epsilon_{yy} = -\frac{\nu\sigma_{zz}}{E} \qquad \epsilon_{zz} = -\frac{\sigma_{zz}}{E}$$

The purpose of this analysis is to find the displacement in z direction. Strains are derivatives of displacement as shown in the generalised Equation 2.7.1:

$$\epsilon_{ij} = \frac{1}{2}\left(\frac{\partial u_i}{\partial x_j} + \frac{\partial u_j}{\partial x_i}\right)$$

Strain in z direction can therefore be written as:

$$\epsilon_{zz} = \frac{\partial u_z}{\partial x_z}$$

Integration of Equation 2.7.1 over height h with respect to z yields:

$$
\begin{aligned}
u_z &= \int_0^h \epsilon_{zz} dz \\
&= \epsilon_{zz} \int_0^h dz \\
&= \epsilon_{zz} h
\end{aligned}
$$

2.7.2 Numerical approach

2.8 Milestone 1: Key Findings

1. Rounding of macro feature layer is caused by inadequate focusing of the projector in relation to the membrane/building plate.
2. Sufficient curing of FunToDo Industrial Blend Red resin can be achieved at 0.5 s exposure time. Higher values of light amplitude results in better curing of part. No over-curing observed even at $LA = 700$.
3. Cleaning procedure proves to have a significant influence on the macro feature layer. A mix of residue isopropyl alcohol and resin agglomerates in corners of the feature layer and leaves unwanted holes or protrusions.
4. QR-codes must have a quiet zone (logic zero) 4X wide on all four sides.

3 Results & Discussion

1. Experiment with different grey scale methods
2. Test more materials
3. HDT tests in OWN GARDEN
4. Print benchmark tests and compare
5. Elaborate grey scale patterning and tests
6. Conformal cooling

4 Conclusion

5 Future Works

References

[AZoM, 2001] AZoM (2001). Stainless steel - grade 420 (uns s42000). https://www.azom.com/article.aspx?ArticleID=6239.Localised09/09/2018. Material Properties Datasheet.

[AZoM, 2012] AZoM (2012). P20 tool steel - low-carbon mold steel uns t51620. https://www.azom.com/article.aspx?ArticleID=6239.Localised09/09/2018. Material Properties Datasheet.

[Denso, 2011] Denso, A. (2011). Qr code essentials. *Denso Wave*, 900.

[EnvisionTec, 2015] EnvisionTec (2015). *Safety Data Sheet according to Regulation (EC) No. 1907/2006 (REACH) for Photopolymer E-Tool Series*. Gladbeck, Germany. https://envisiontec.com/3d-printing-materials/micro-materials/e-tool-2-0/.. Localised 09/09/2018.

[EnvisionTec, 2016] EnvisionTec (2016). *E-Tool 2.0 Technical Datasheet*. Gladbeck, Germany. https://envisiontec.com/3d-printing-materials/micro-materials/e-tool-2-0/.. Localised 09/09/2018.

[Formlabs, 2016] Formlabs, I. (2016). *SAFETY DATA SHEET for High Temp Photoreactive Resin for Form 1+, Form 2*, version 1 edition. https://formlabs.com/media/upload/HighTemp-DataSheet.pdf. Localised 09/09/2018.

[Formlabs, 2017] Formlabs, I. (2017). *High Temp Material Data Sheet*, flhtam01 edition. https://formlabs.com/media/upload/HighTemp-DataSheet.pdf. Localised 09/09/2018.

[Granta Design Limited, 2018] Granta Design Limited (2018). CES Edupack 2018. "http://www.grantadesign.com/education/edupack/index.htm. Version: 18.1.1. Localised 12/09/2018.

[Hara et al., 1998] Hara, M., Watabe, M., Nojiri, T., Nagaya, T., and Uchiyama, Y. (1998). Optically readable two-dimensional code and method and apparatus using the same. US Patent 5,726,435.

[ISO/IEC, 2015] ISO/IEC (2015). Information technology automatic identification and data capture techniques qr code bar code symbology specification. *International Organization for Standardization, ISO/IEC*, 18004.

[Leo and Cuvelliez, 1996] Leo, V. and Cuvelliez, C. (1996). The effect of the packing parameters, gate geometry, and mold elasticity on the final dimensions of a molded part. 36:1961–1971.

[PolyOne Cooperation, 1996] PolyOne Cooperation (1996). Tool steel recommendations for injection molds. http://www.polyone.com/files/resources/TSR12_Tool_Steel_Recommendations_for_Injection_Molds_Designed_for_Processing_Geon_Vinyl_Compounds.pdf.Localised09/09/2018. Technical Service Report.

[Tarjan et al., 2014] Tarjan, L., Šenk, I., Tegeltija, S., Stankovski, S., and Ostojic, G. (2014). A readability analysis for qr code application in a traceability system. *Computers and Electronics in Agriculture*, 109:1 – 11.

6 Appendix